Drivers of summer extreme temperature trends in Europe: insight from three major heat waves using flow analogues

SUPPORTING INFORMATION

Luca Famooss Paolini [a], Salvatore Pascale [a], Paolo Ruggieri [a], Erika Brattich [a], Silvana Di Sabatino [a]

[a] *Department of Physics and Astronomy "Augusto Righi", University of Bologna, Bologna, Italy*

Corresponding author: Luca Famooss Paolini, luca.famoosspaolini@unibo.it

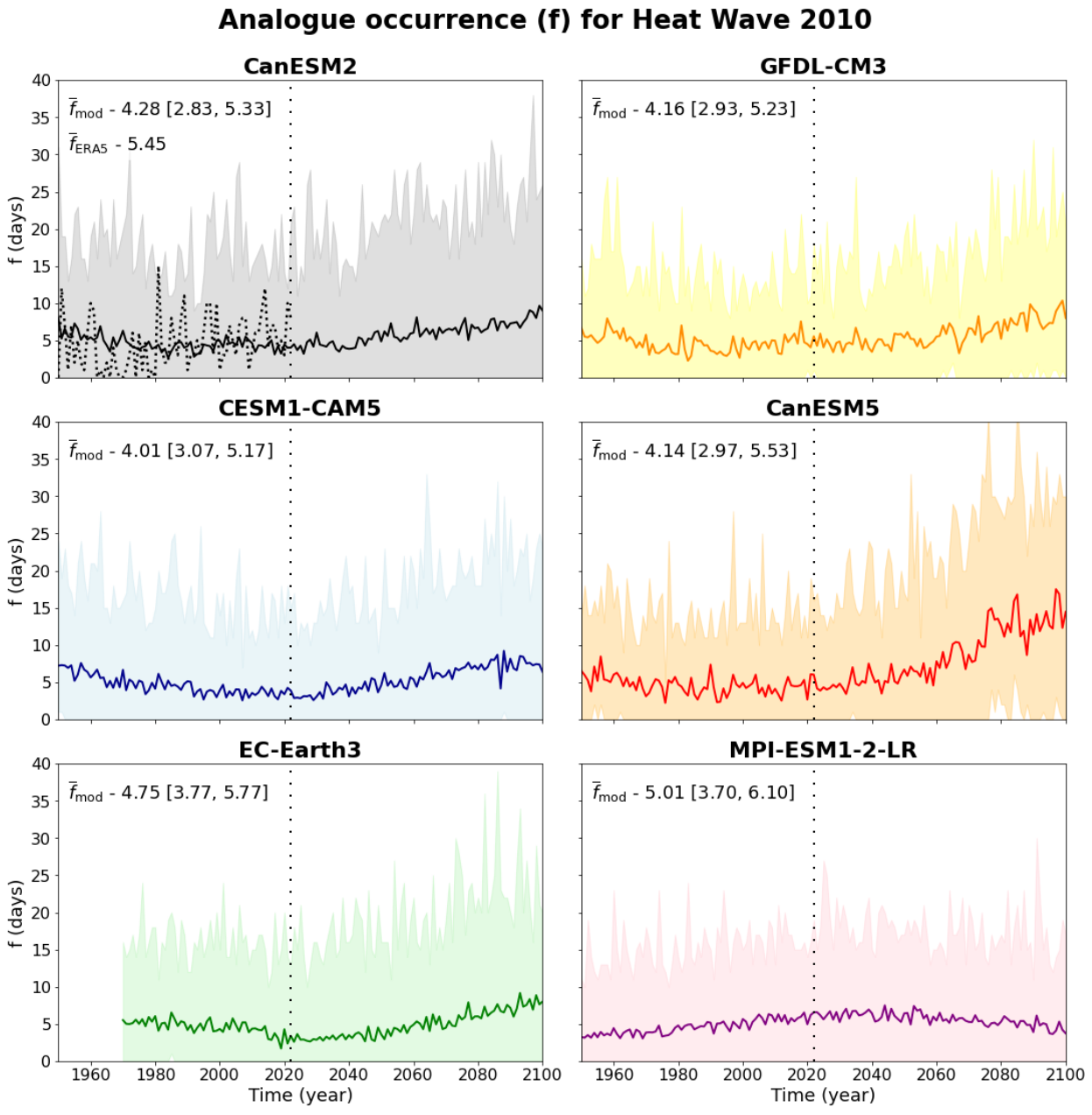

FIG. S1. Occurrence of summer atmospheric analogues (f) for the 2010 Russian heat wave in ERA5 and models. For each model, the solid line shows the model mean analogue occurrence, while the shaded envelope indicates the spread across ensemble members. In the CanESM2 panel (top left), ERA5 is shown as a black dashed line. Numbers reported in the upper-left corner of each panel correspond to the climatological analogue occurrence during the reference period 1981–2010: $\overline{f}_{mod}$ for the model mean, with brackets indicating the range across members, and $\overline{f}_{ERA5}$ for ERA5. The vertical dotted line marks the transition between the historical (1950–2022) and projection (2023–2100) periods.

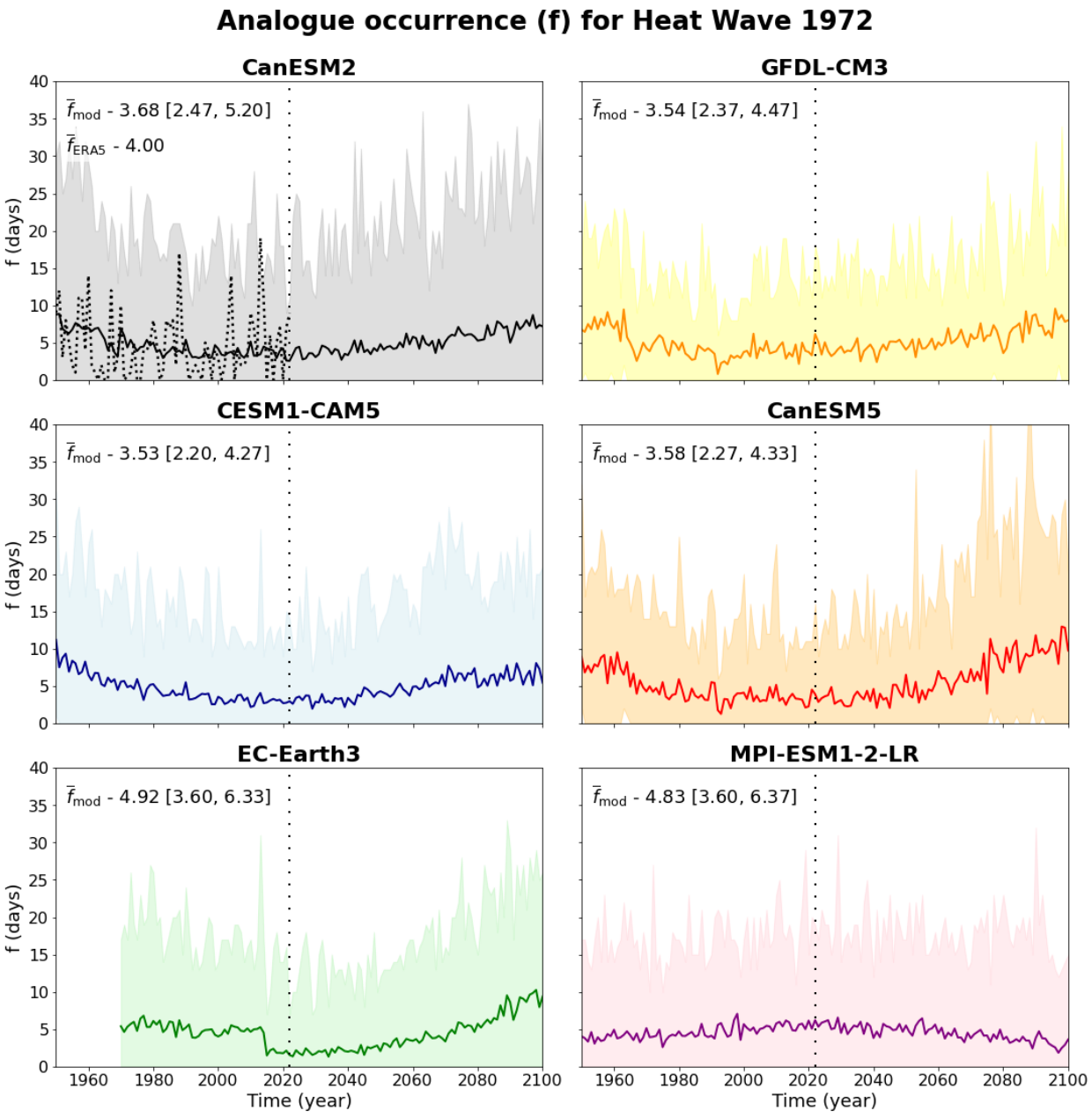

FIG. S2. Same as Figure S1, but for the 1972 Scandinavian heat wave.

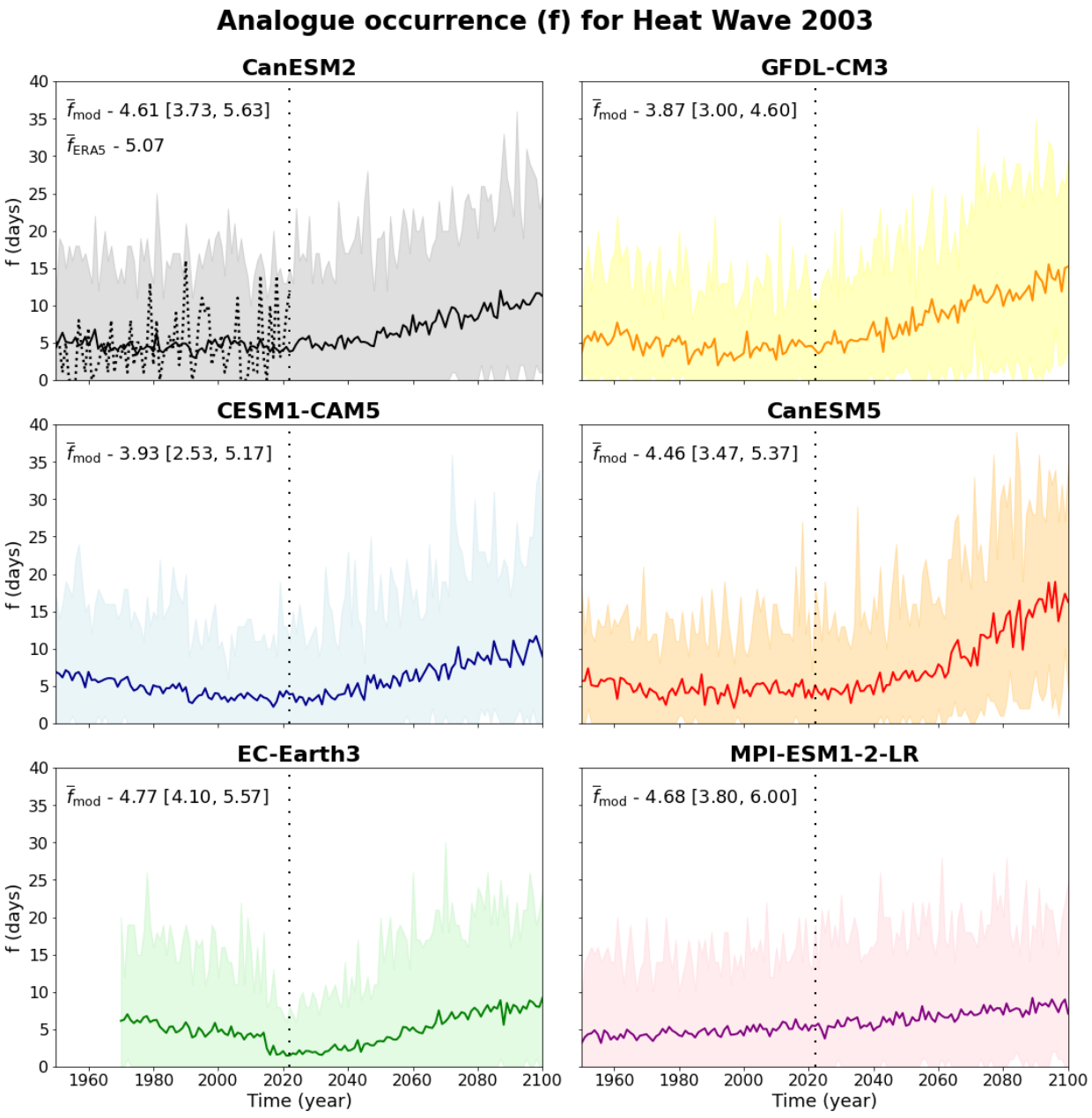

FIG. S3. Same as Figure S1, but for the 2003 French heat wave.

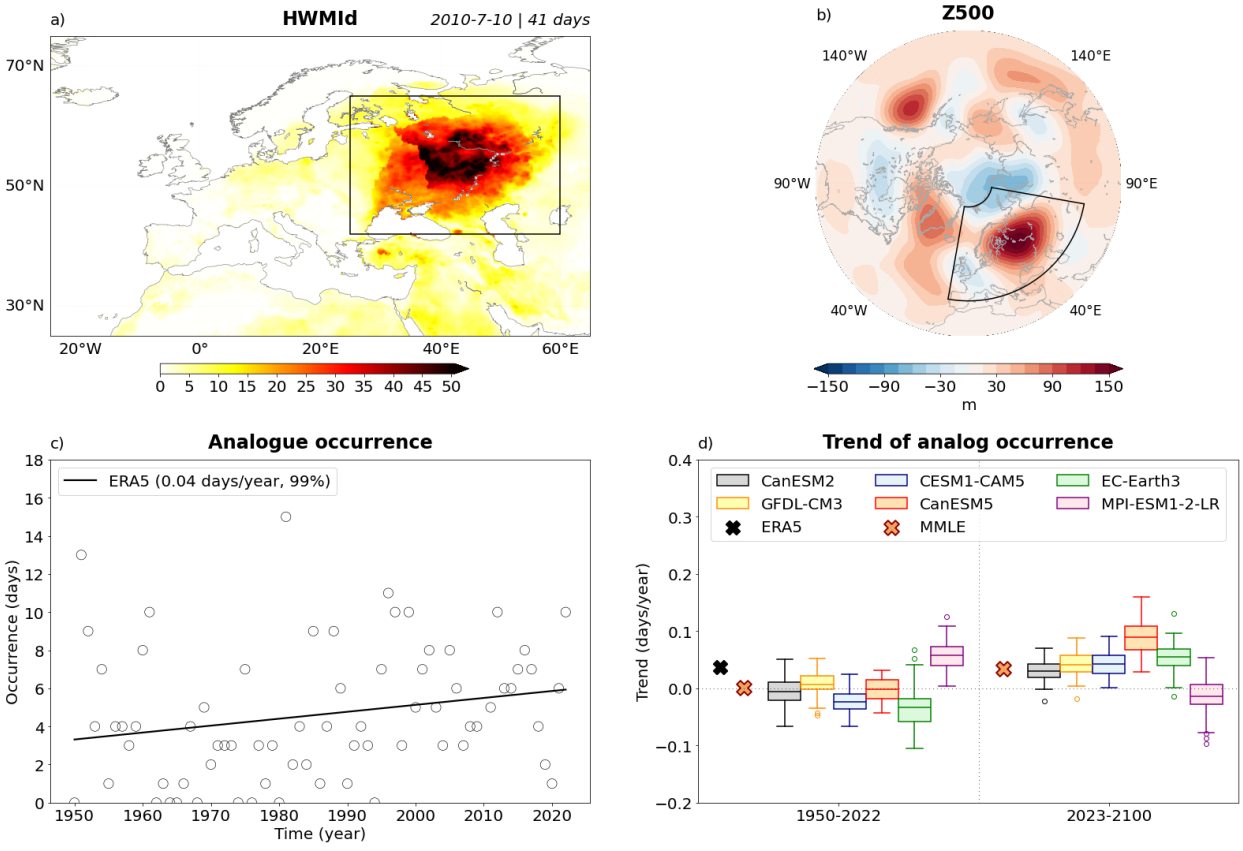

FIG. S4. a) HWMId for the 2010 Russian heat wave in ERA5. The starting date and the duration of the heat wave are shown on the top right corner. The black box (25°W–60°W; 42°N–65°N) marks the region where the partition trend analysis is conducted for this heat wave. Please, refer to section 2d for more details about this analysis. b) Z500 anomalies associated with the 2010 Russian heat wave, in the ERA5 dataset. These anomalies are calculated as daily Z500 departures from the 1981–2010 reference time period and averaged along the whole duration of the heat wave. The black box (10°W–80°E; 40°N–80°N) marks the region where the flow analogue technique is conducted for this heat wave. Refer to section 2c for more details about this analysis. c) Occurrence of summer analogues (days; black circles) of the 2010 Russian heat wave atmospheric circulation, in the ERA5 dataset during the historical period (1950–2022). The black line represents the linear trend in analogue occurrence (days year^{-1}), with the trend value and its statistical significance provided in the upper left corner. d) Trend of analogue occurrence (days year^{-1}) for ERA5 (black cross), MMLE mean (red cross) and single models (colored boxplots) during the historical (1950–2022) and projection (2023–2100) periods. The boxplots display the interquartile range, with the model mean indicated by the horizontal line inside each box. The whiskers extend to 1.5 times the interquartile range, and any outliers beyond this range are shown as individual circles.

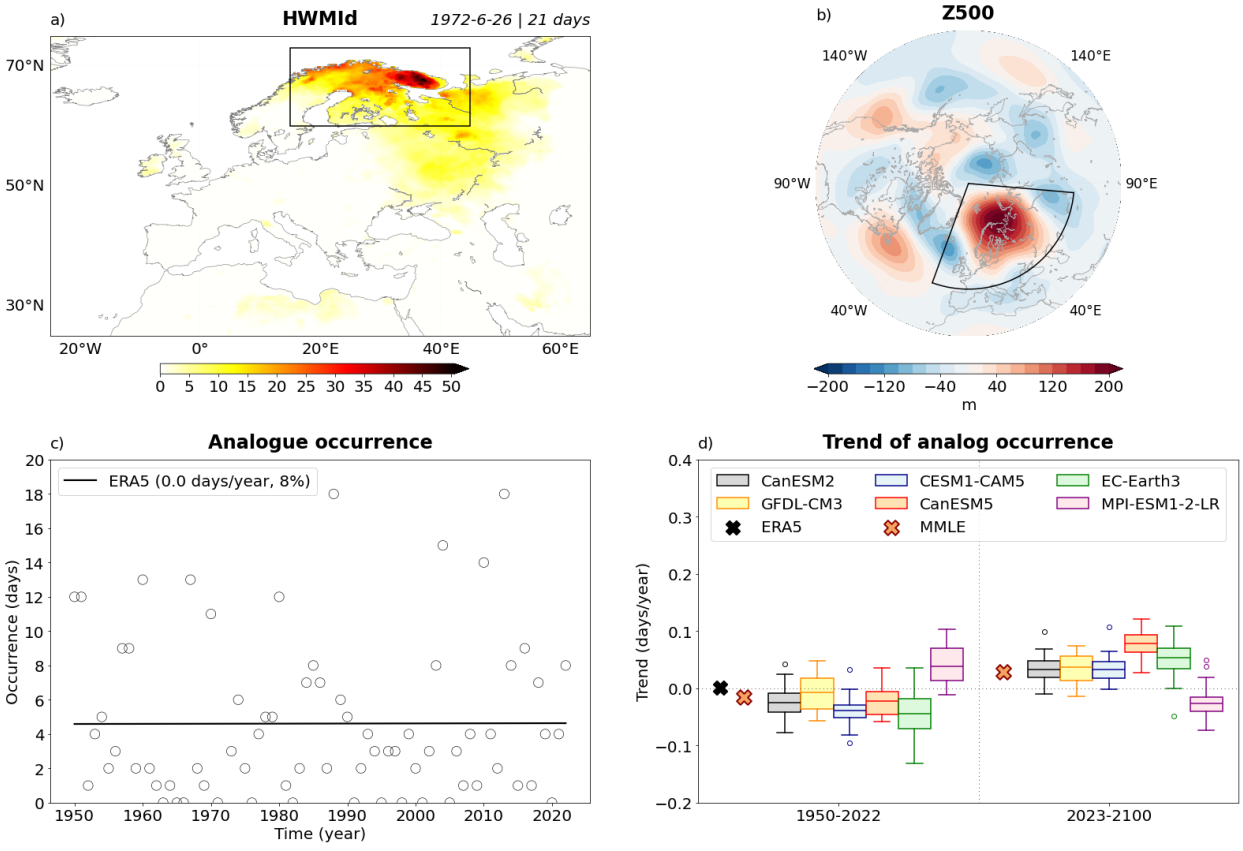

FIG. S5. Same as Figure S4, but for the 1972 Scandinavian heat wave. In this case, the black box in a) has coordinates 15°E–45°E and 60°N–73°N, while the black box in b) has coordinates 20°W–85°E and 45°N–90°N.

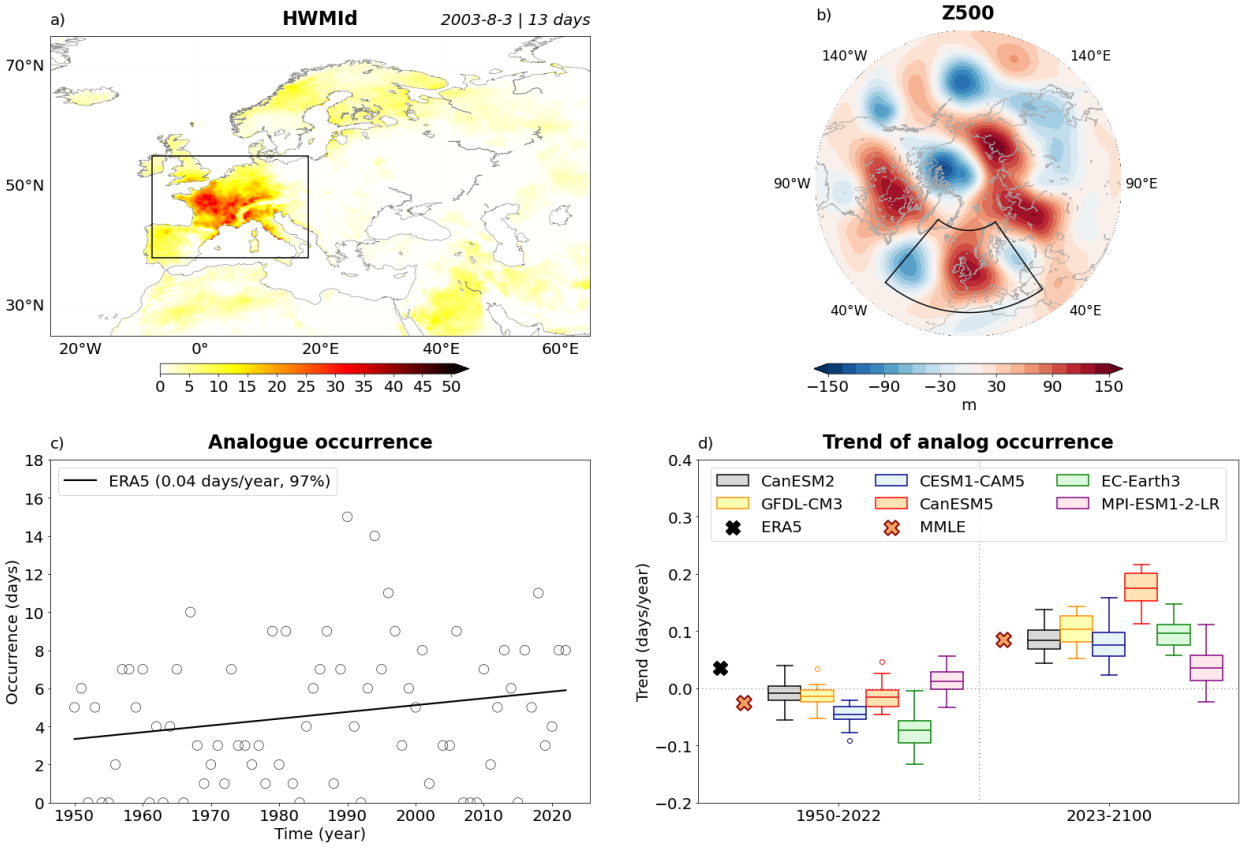

FIG. S6. Same as Figure S4, but for the 2003 French heat wave. In this case, the black box in a) has coordinates 8°W–18°E and 38°N–55°N, while the black box in b) has coordinates 40°W–35°E and 35°N–70°N.

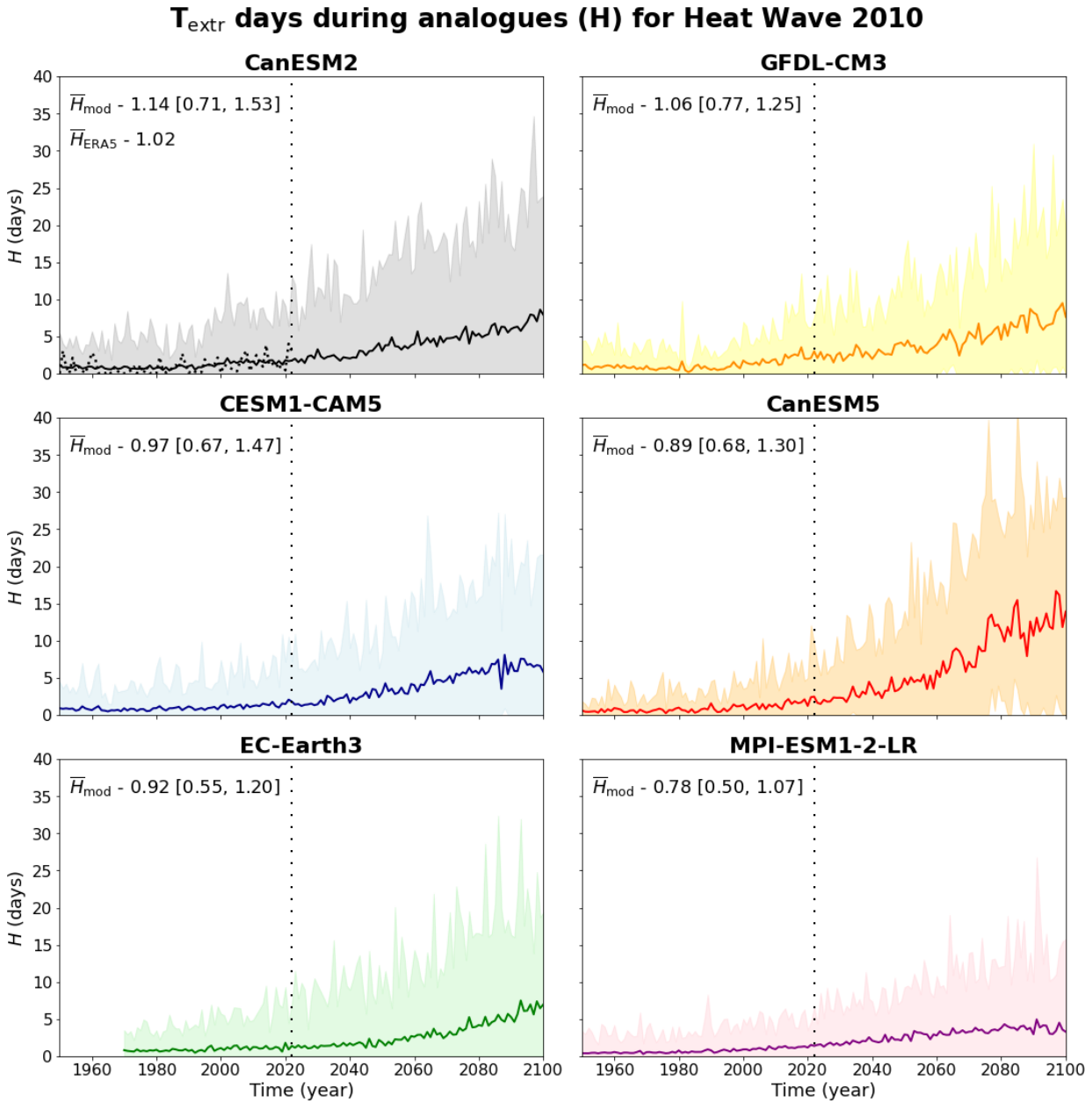

FIG. S7. Occurrence of summer extreme temperature days during the atmospheric analogues (H) of the 2010 Russian heat wave. For each model, the solid line shows the model mean value of H, while the shaded envelope indicates the spread across ensemble members. In the CanESM2 panel (top left), ERA5 is shown for reference as a black dashed line. Numbers reported in the upper-left corner of each panel correspond to the climatological H during the reference period 1981–2010: $\overline{H}_{mod}$ for the model mean, with brackets indicating the range across members, and $\overline{H}_{ERA5}$ for ERA5. The vertical dotted line marks the transition between the historical (1950–2022) and projection (2023–2100) periods.

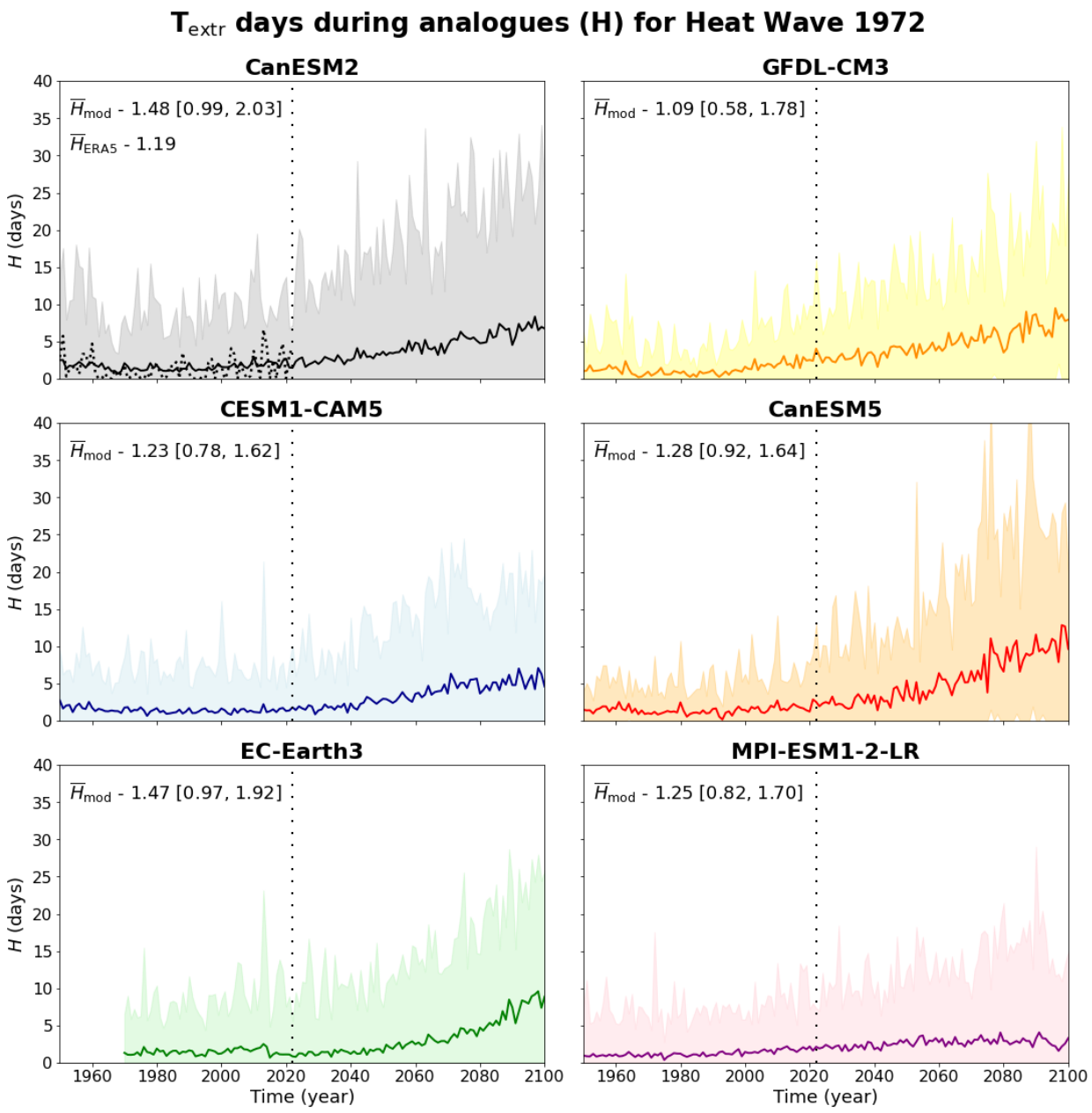

FIG. S8. Same as Figure S7, but for the 1972 Scandinavian heat wave.

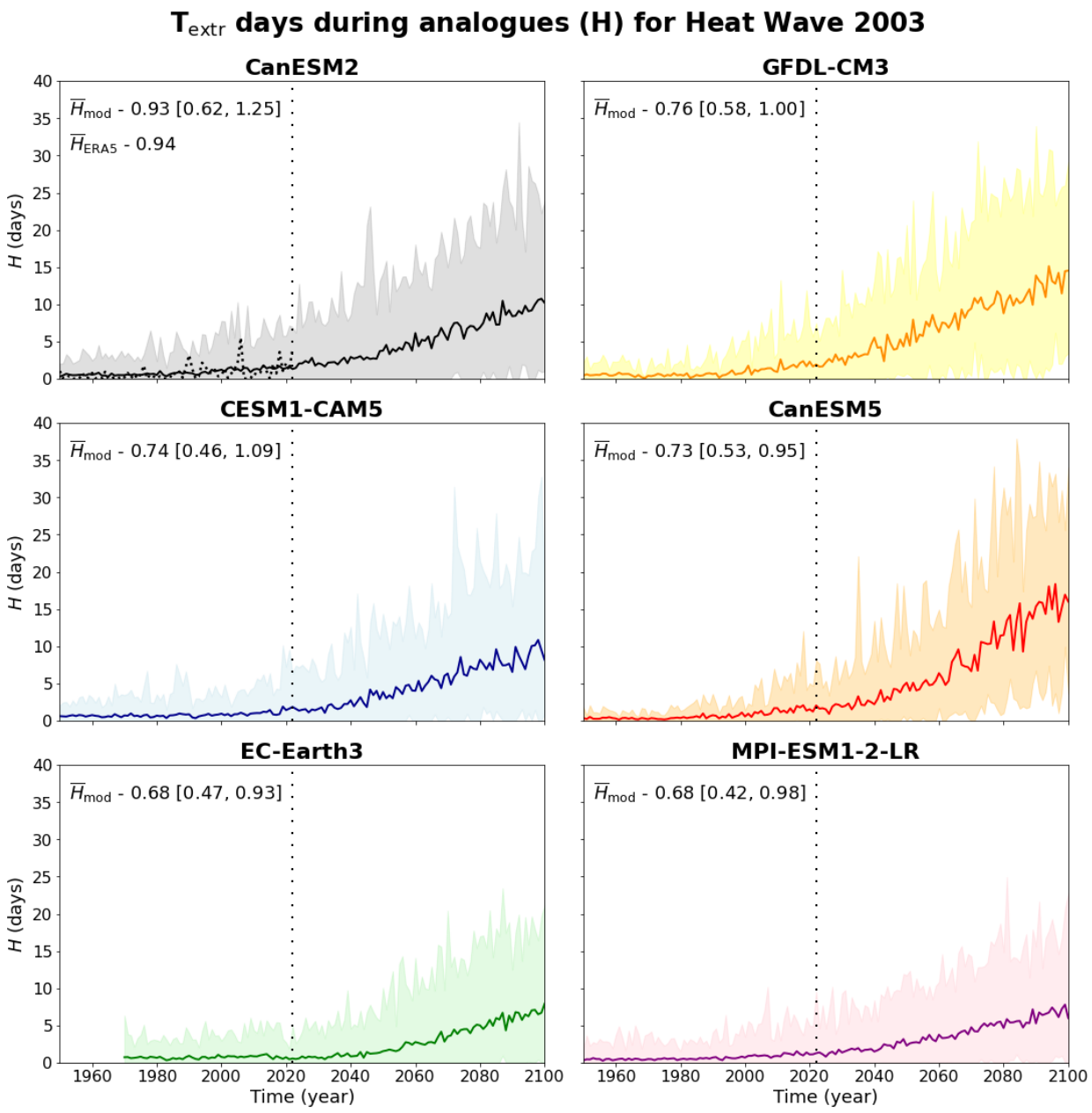

FIG. S9. Same as Figure S7, but for the 2003 French heat wave.

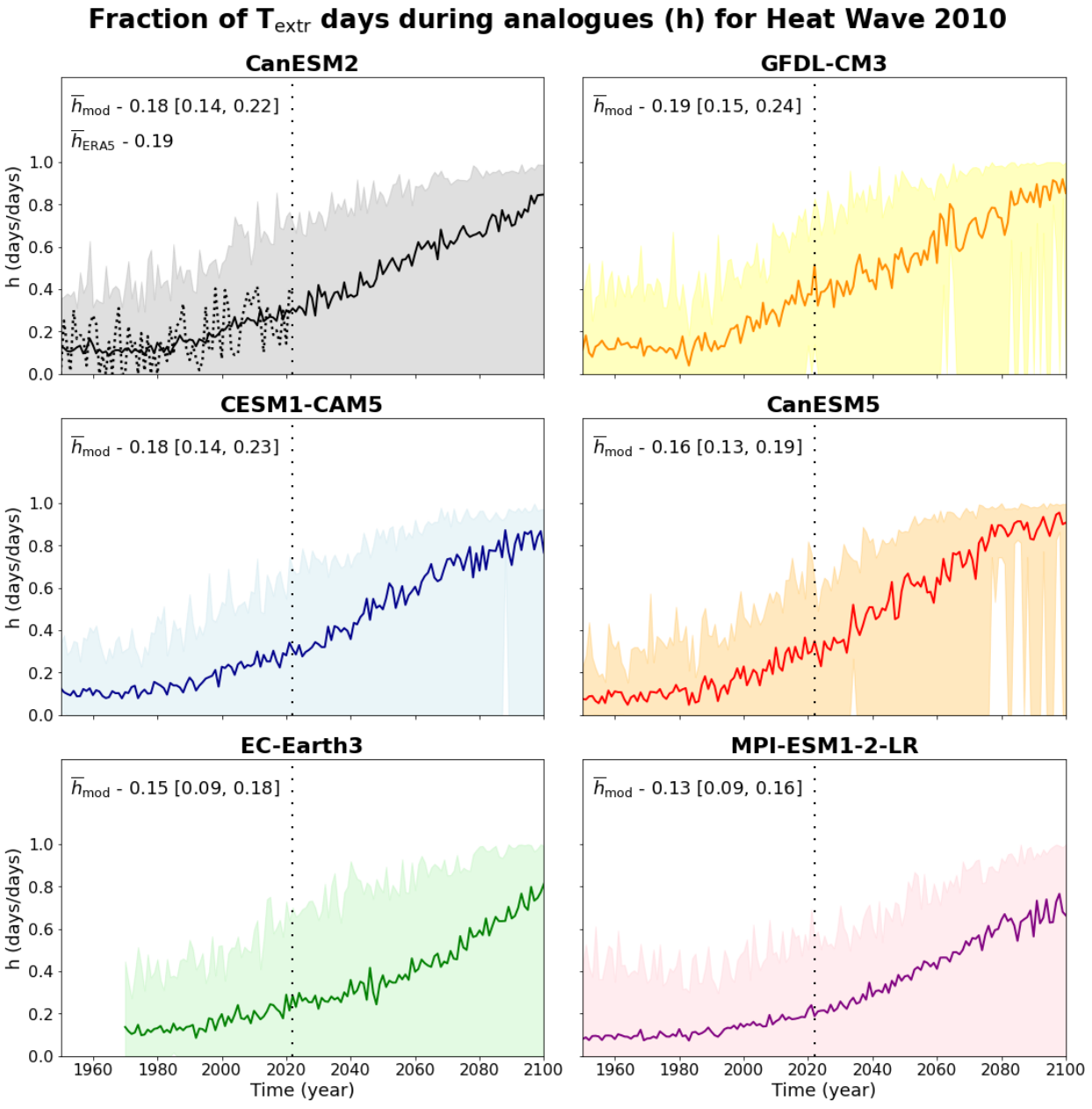

FIG. S10. Fraction of summer extreme temperature days occurring during the atmospheric analogues (h) for the 2010 Russian heat wave. For each model, the solid line shows the model mean value of h, while the shaded envelope indicates the spread across ensemble members. In the CanESM2 panel (top left), ERA5 is shown for reference as a black dashed line. Numbers reported in the upper-left corner of each panel correspond to the climatological h during the reference period 1981–2010: $\overline{h}_{mod}$ for the model mean, with brackets indicating the range across members, and $\overline{h}_{ERA5}$ for ERA5. The vertical dotted line marks the transition between the historical (1950–2022) and projection (2023–2100) periods.

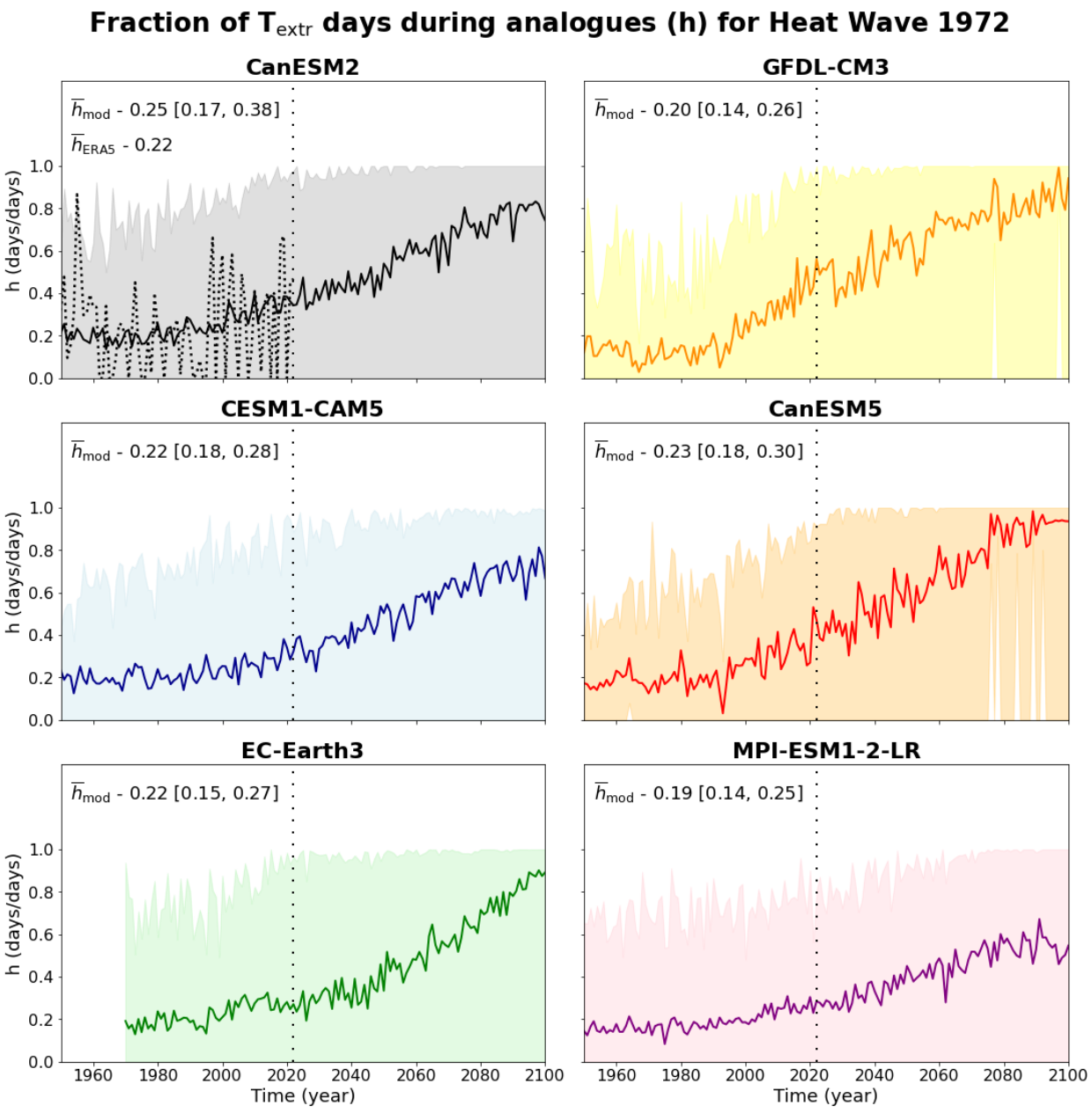

FIG. S11. Same as Figure S10, but for the 1972 Scandinavian heat wave.

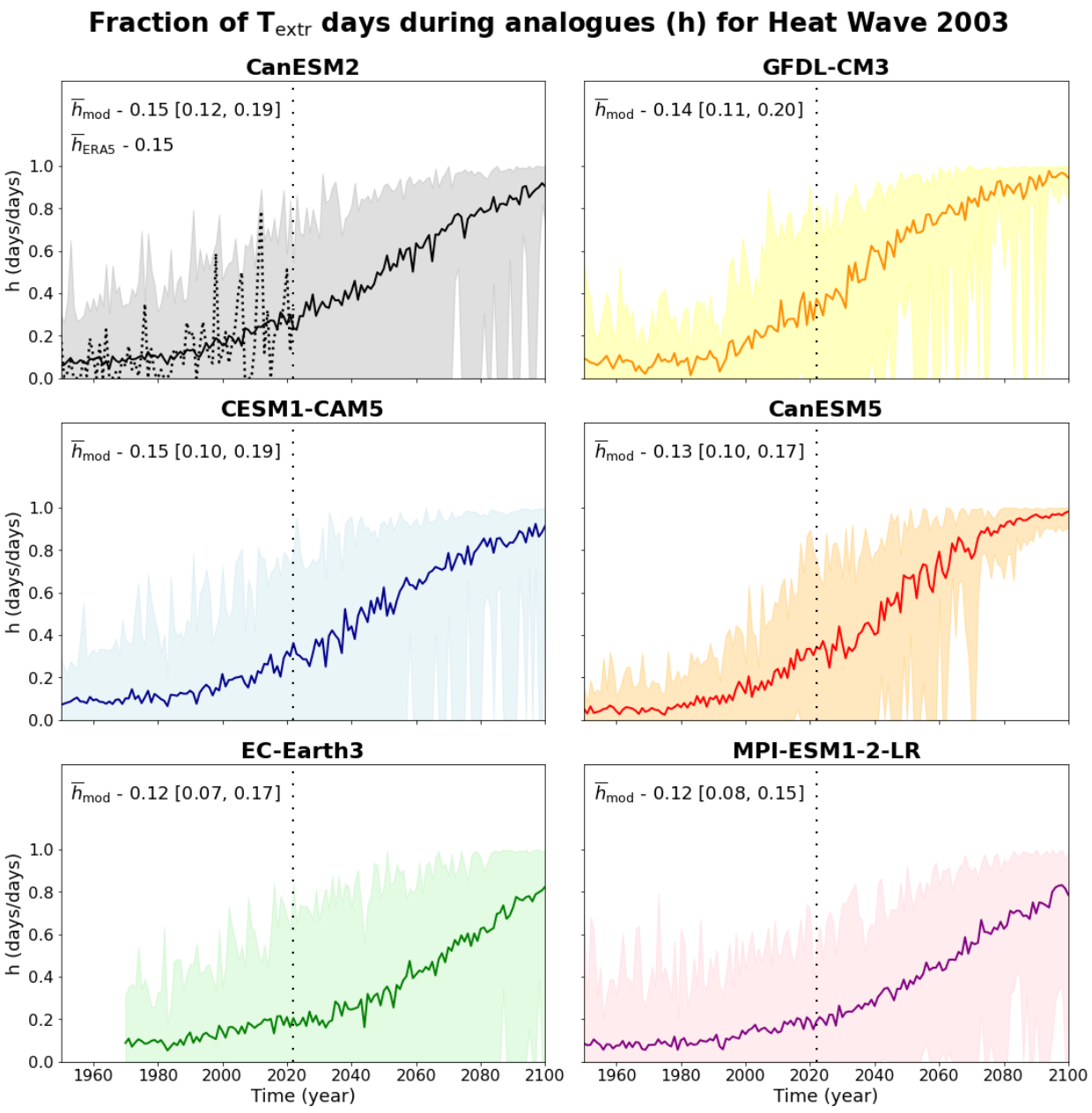

FIG. S12. Same as Figure S10, but for the 2003 French heat wave.

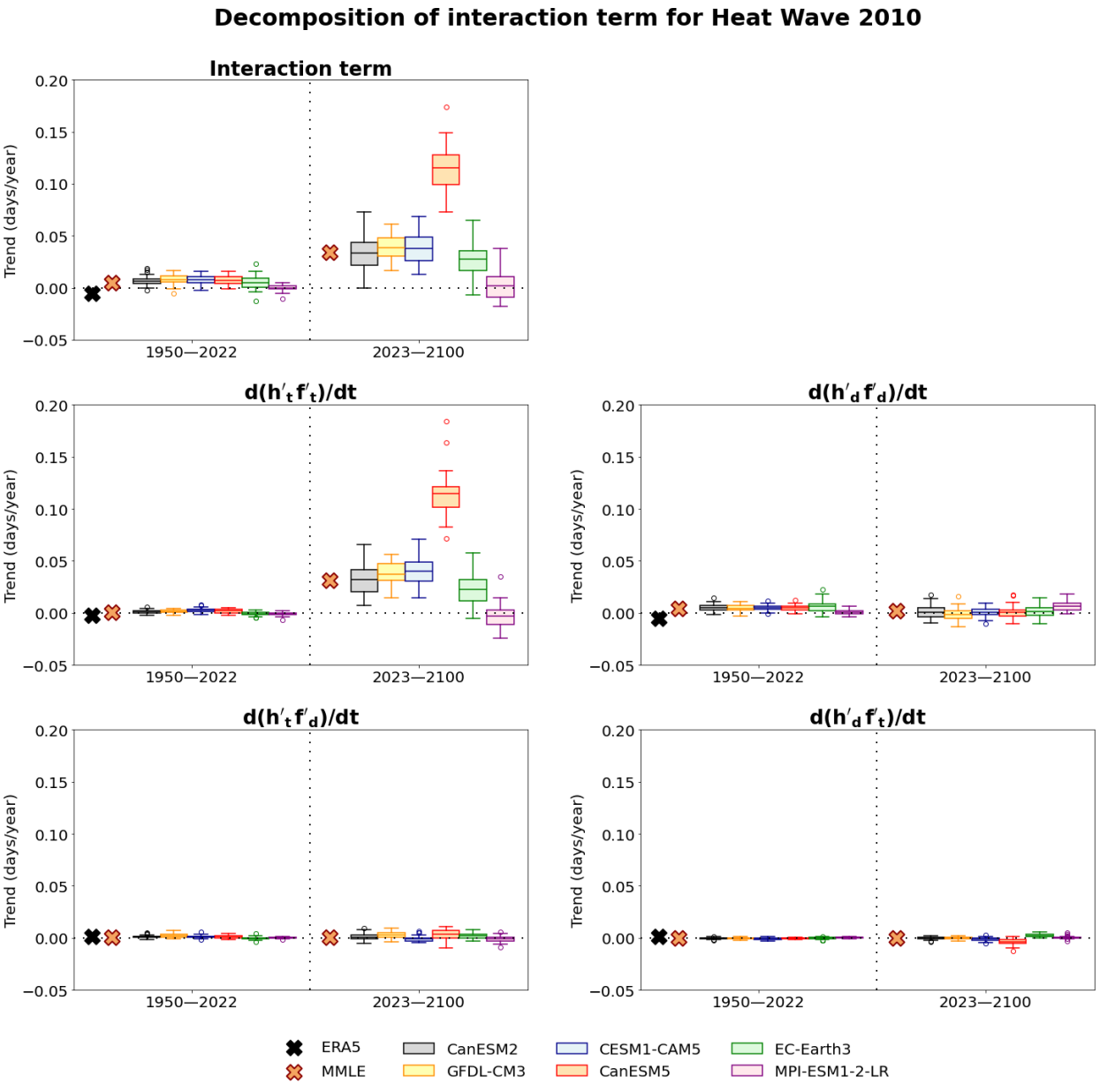

FIG. S13. Decomposition of the interaction term (days year^{-1}) for the 2010 Russian heat wave. Top left: interaction term; central left: $\frac{d(h'_t f'_t)}{dt}$; central right: $\frac{d(h'_d f'_d)}{dt}$; bottom left: $\frac{d(h'_t f'_d)}{dt}$; bottom right: $\frac{d(h'_d f'_t)}{dt}$. Trends are calculated for the historical period (1950–2022) for ERA5 (black cross), the MMLE mean (red cross) and individual models (colored boxplots), and for the projection period (2023–2100) for MMLE mean and individual models. The boxplots display the interquartile range, with the model mean indicated by the horizontal line inside each box. The whiskers extend to 1.5 times the interquartile range, and any outliers beyond this range are shown as individual circles.

TABLE S1. Decomposition of the interaction term (days year^{-1}) for the 2010 French heat wave. Columns report the full interaction term and its four components, $\frac{d(h'_t f'_t)}{dt}$, $\frac{d(h'_d f'_d)}{dt}$, $\frac{d(h'_t f'_d)}{dt}$, and $\frac{d(h'_d f'_t)}{dt}$, for both the historical and projection periods. For each model and the MMLE, the single components are expressed as percentages of the corresponding ensemble mean interaction term.

	1950–2022					**2023–2100**				
	Interaction term (days year^{-1})	$\frac{d(h'_t f'_t)}{dt}$ (%)	$\frac{d(h'_d f'_d)}{dt}$ (%)	$\frac{d(h'_t f'_d)}{dt}$ (%)	$\frac{d(h'_d f'_t)}{dt}$ (%)	Interaction term (days year^{-1})	$\frac{d(h'_t f'_t)}{dt}$ (%)	$\frac{d(h'_d f'_d)}{dt}$ (%)	$\frac{d(h'_t f'_d)}{dt}$ (%)	$\frac{d(h'_d f'_t)}{dt}$ (%)
ERA5	-0.006	47.45	95.09	-19.47	-23.07	-	-	-	-	-
CanESM2	0.007	16.96	72.57	16.10	-5.62	0.034	95.70	2.37	2.25	-0.32
GFDL-CM3	0.008	19.64	58.28	27.97	-5.89	0.039	96.98	-4.01	6.96	0.07
CESM1-CAM5	0.008	31.88	65.76	13.40	-11.04	0.038	104.22	1.41	-2.59	-3.05
CanESM5	0.007	22.00	67.15	17.06	-6.21	0.115	99.59	0.42	3.13	-3.14
EC-Earth3	0.005	-12.04	124.76	-8.78	-3.94	0.028	81.11	4.54	6.63	7.72
MPI-ESM1-2-LR	-0.000	1777.68	-788.87	-161.89	-726.92	0.002	-173.13	324.30	-60.36	9.79
MMLE	0.005	11.06	81.06	12.28	-4.92	0.034	92.42	5.45	2.16	-0.02

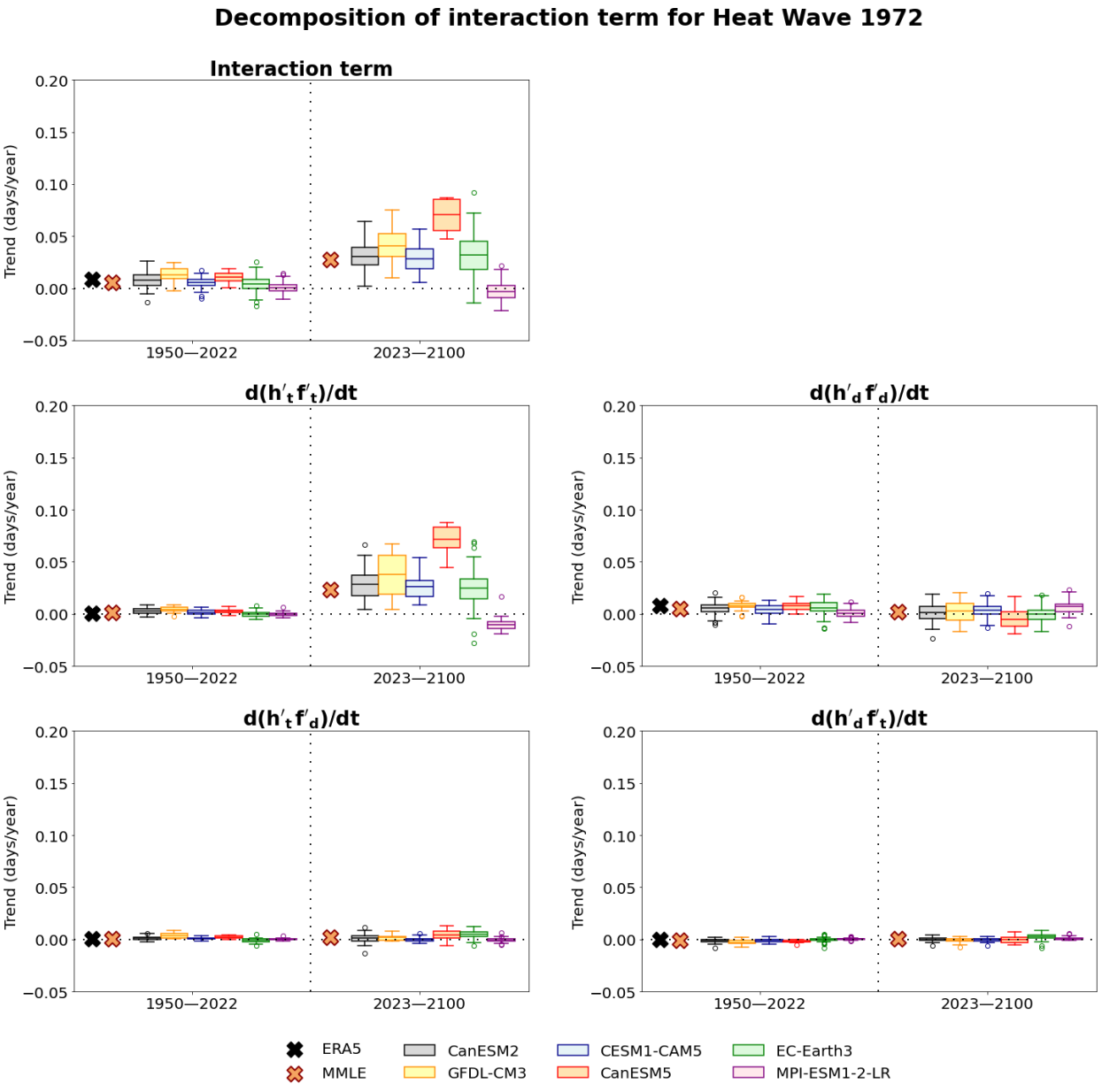

FIG. S14. Same as Figure S13, but for the 1972 Scandinavian heat wave.

TABLE S2. Same as Table S1, but for the 1972 Scandinavian heat wave.

	1950–2022					2023–2100				
	Interaction term (days year^{-1})	$\frac{d(h'_t f'_t)}{dt}$ (%)	$\frac{d(h'_d f'_d)}{dt}$ (%)	$\frac{d(h'_t f'_d)}{dt}$ (%)	$\frac{d(h'_d f'_t)}{dt}$ (%)	Interaction term (days year^{-1})	$\frac{d(h'_t f'_t)}{dt}$ (%)	$\frac{d(h'_d f'_d)}{dt}$ (%)	$\frac{d(h'_t f'_d)}{dt}$ (%)	$\frac{d(h'_d f'_t)}{dt}$ (%)
ERA5	0.009	3.81	90.97	5.75	-0.53	-	-	-	-	-
CanESM2	0.008	31.51	66.76	16.79	-15.06	0.030	91.95	4.30	3.92	-0.17
GFDL-CM3	0.013	32.97	61.04	26.44	-20.45	0.041	91.75	5.85	4.30	-1.90
CESM1-CAM5	0.005	29.36	71.30	15.92	-16.58	0.029	90.98	11.67	-1.16	-1.49
CanESM5	0.011	25.78	73.57	18.95	-18.30	0.071	101.52	-7.34	5.93	-0.11
EC-Earth3	0.004	-11.77	131.74	-19.45	-0.52	0.032	77.20	-0.89	15.58	8.11
MPI-ESM1-2-LR	0.001	-81.48	107.00	24.81	49.67	0.003	320.97	-214.95	16.83	-22.85
MMLE	0.006	20.46	79.15	13.22	-12.83	0.028	84.24	7.30	6.32	2.14

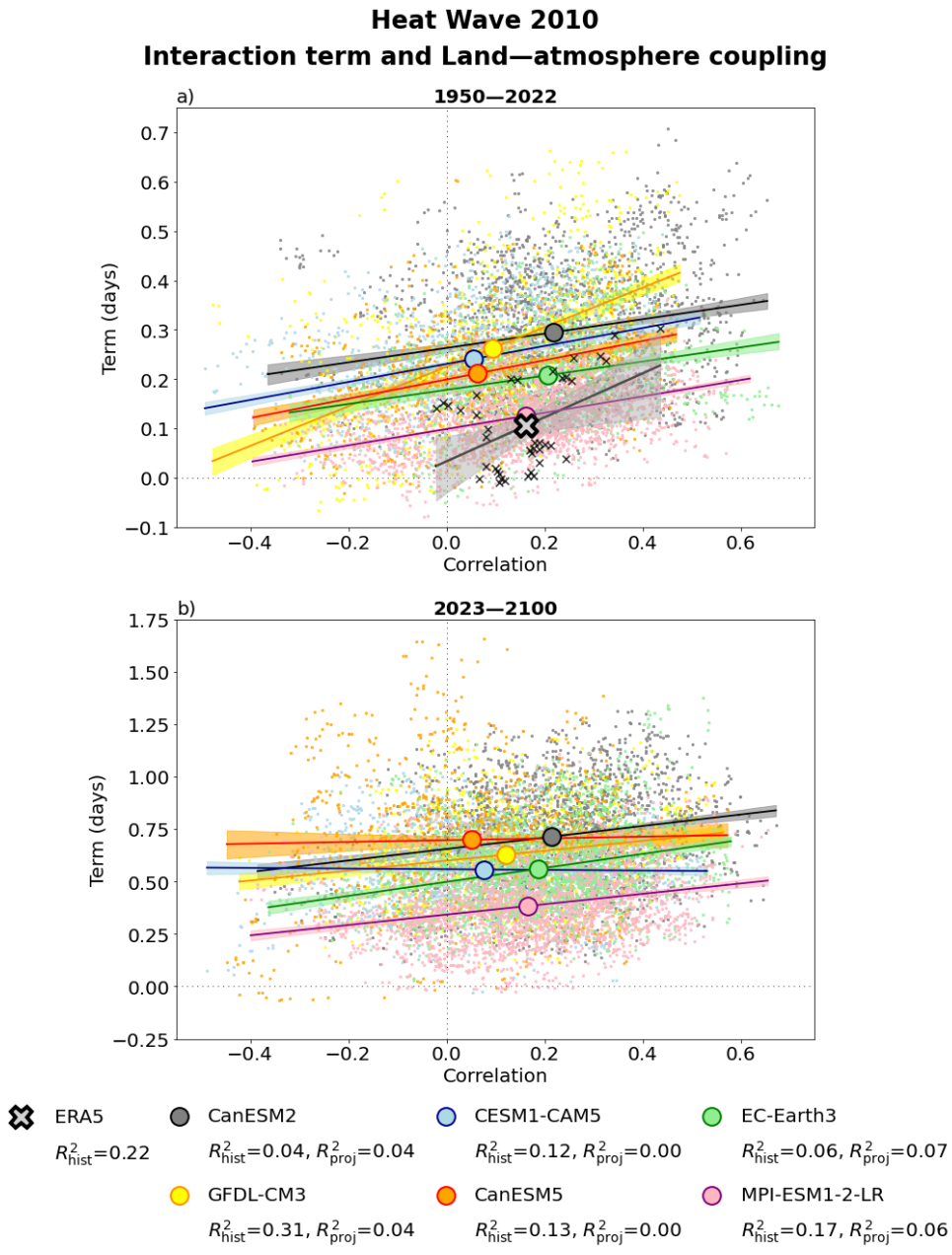

FIG. S15. a) Scatterplot relating the $h'_d \cdot f'_d$ product (days^{-1}) to land–atmosphere coupling during the historical period (1950–2022) for the 2010 Russian heat wave. The land–atmosphere coupling is assessed through the correlation between the summer SHF and analogue occurrence using a 30-year running window, and is paired with the mean value of the $h'_d \cdot f'_d$ product over the same window. Results are shown for individual model members during each 30-year window (small circles) and for model means (large circles). Solid lines denote the least squares regression between the correlation and the $h'_d \cdot f'_d$ product. Shaded areas indicate the 95% confidence interval of the regression, based on a bootstrap test performed 1000 times. The coefficient of determination (R^2) is reported in the legend for each dataset as a measure of the fraction of $h'_d \cdot f'_d$ variance explained by the land–atmosphere coupling. b) Same as a), but for the projection period (2023–2100).

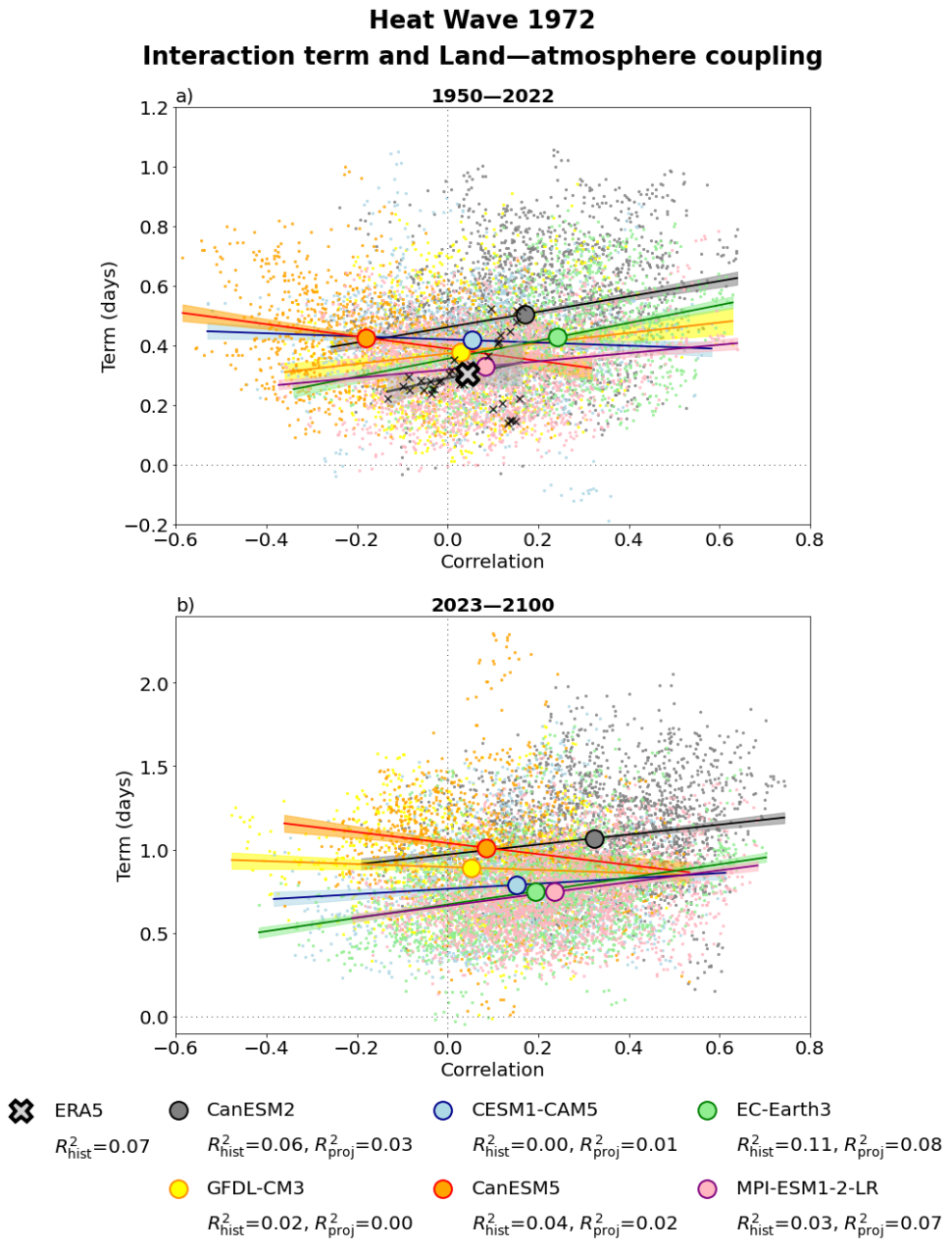

FIG. S16. Same as Figure S15, but for the 1972 Scandinavian heat wave.